# Supplementary Information

## Catalysts derived from earth-abundant natural biomass enable efficient photocatalytic CO2 conversion for achieving a closed-loop carbon cycle

Qi-Su Huang,[a] Wei Wei,[b] Bing-Jie Ni [b,*]

[a] State Key Laboratory of Pollution Control and Resources Reuse, College of Environmental Science and Engineering, Tongji University, Shanghai 200092, P.R. China

[b] Centre for Technology in Water and Wastewater, School of Civil and Environmental Engineering, University of Technology Sydney, Sydney, NSW 2007, Australia

***Corresponding Author**

Prof. Bing-Jie Ni

E-mail: bingjieni@gmail.com

**The following are included as supplementary information for this paper:**

**Supplementary Figure**

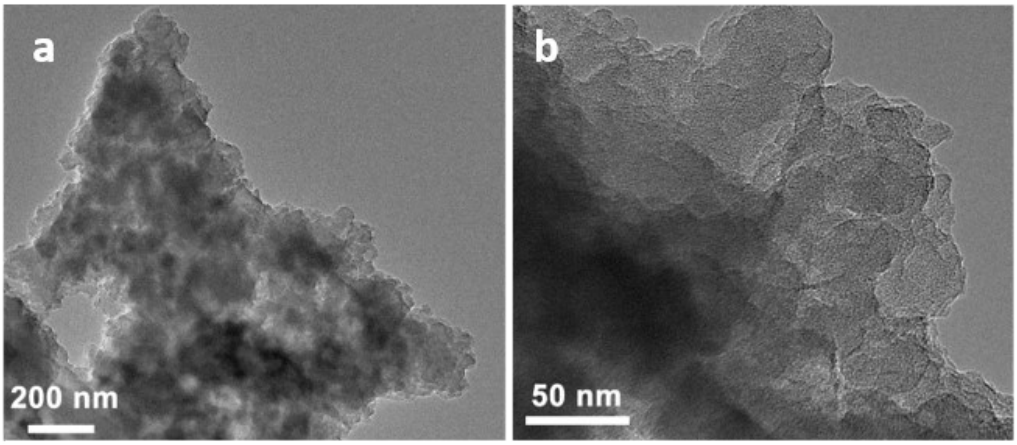


**Supplementary Figure 1.** TEM images at different magnifications of the CKB-3 photocatalyst.

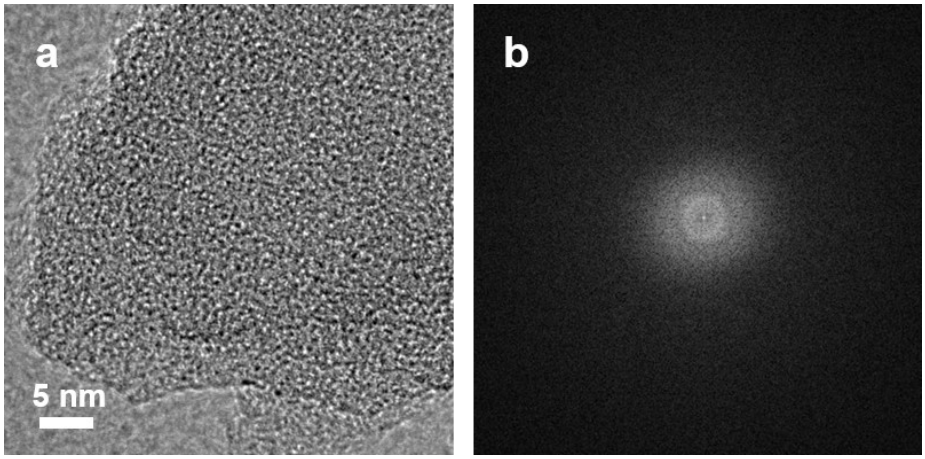


**Supplementary Figure 2.** a) High-resolution TEM image of the CKB-3 photocatalyst and b) the corresponding Fourier transform diffraction pattern.

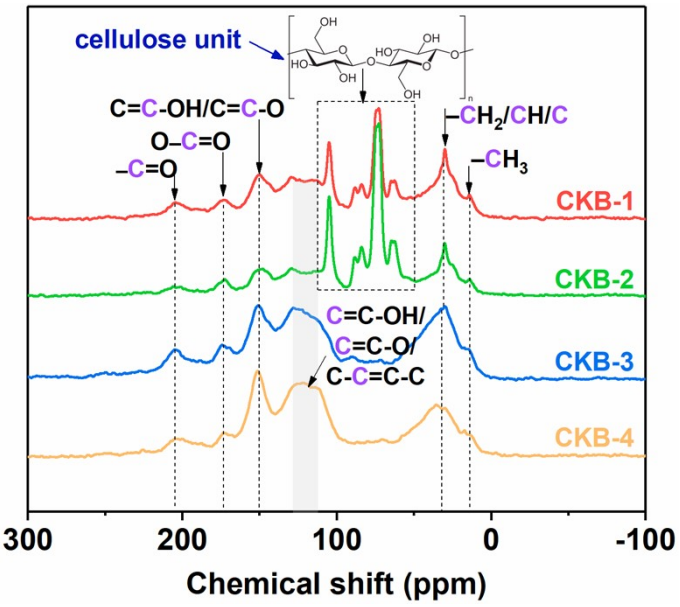


**Supplementary Figure 3.** The $^{13}C$ solid NMR spectra of the CKB photocatalysts.

As seen in **Supplementary Fig. 3**, the typical signals of the anhydro glucose units of the cellulose can be observed in the region of 55−110 ppm for the CKB-1 and the CKB-2[1]. This phenomenon coincides well with the XRD spectra that the crystalline cellulose fails to be eliminated at low concentration of sulfuric acid. In general, the NMR spectra can be briefly divided into three regions: 1) aliphatic carbon in the range of 0−90 ppm, such as the $-CH_3$ at 14 ppm and the $-CH_2$/CH/C at 31 ppm; 2) aromatic carbon in the range of 90−155 ppm, including the conjugated C=C at 110−130 ppm and the C−O at 150 ppm; 3) the region of C=O in the range of 155−220 ppm, containing the O=C−O at 173 ppm and the −C=O at 205 ppm[2,3]. The signals of the aromatic domain are dramatically enhanced in the CKB-3 and CKB-4, implying the formation of concentrated polyaromatic structure in the materials. It can also be seen that abundant oxygen-containing groups, such as the carboxyl, ketone, phenol, quinone, are grafted on the carbon skeleton of the CKB photocatalysts.

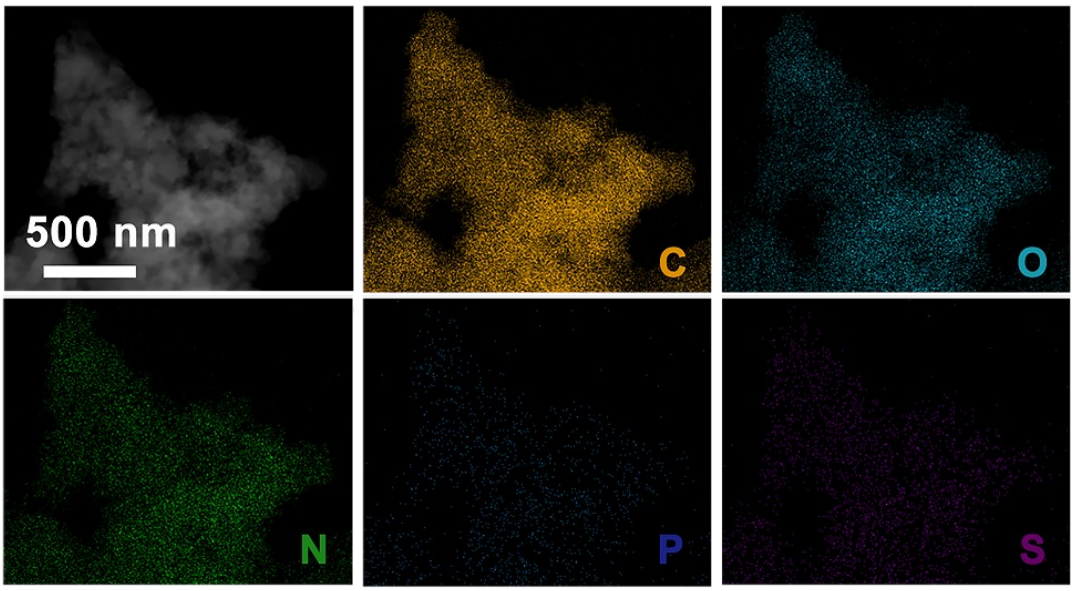


**Supplementary Figure 4.** HRTEM image and the corresponding elemental mappings of the CKB-3.

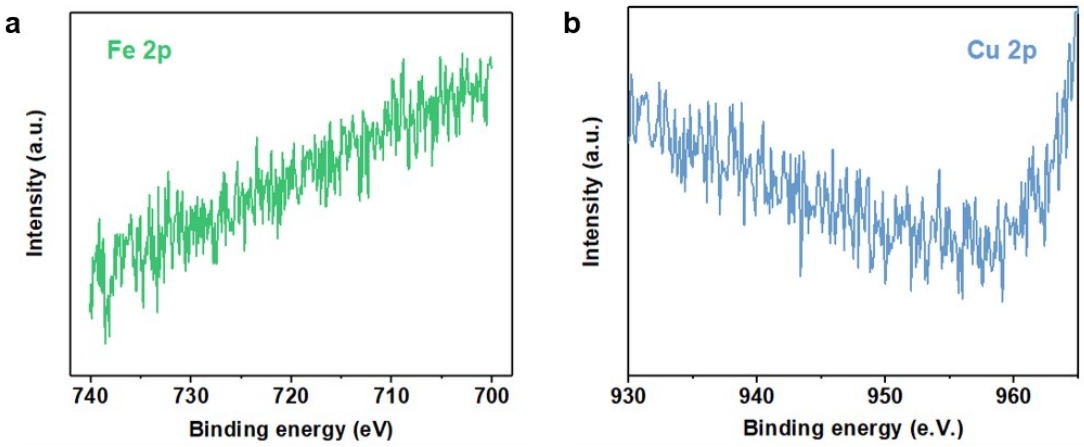


**Supplementary Figure 5.** High-resolution XPS spectra of the a) Fe 2p and b) Cu 2p for the CKB-1.

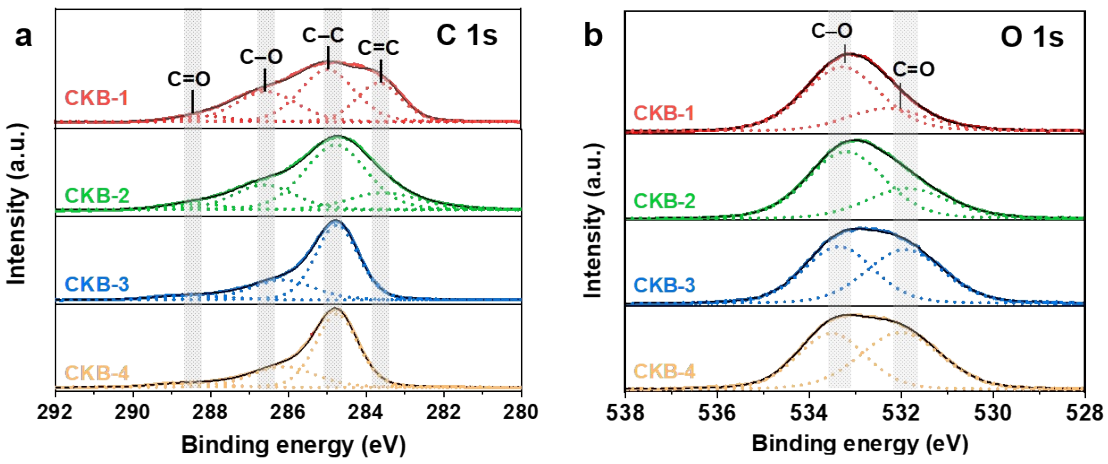


**Supplementary Figure 6.** High-resolution XPS spectra of the a) C 1s and b) O 1s for the CKB photocatalysts

**Supplementary Fig. 6** illustrates the deconvolution of the C 1s and O 1s XPS spectra of the CKB photocatalysts. As shown in **Supplementary Fig. 6a**, the CKB-1 and CKB-2 compose of four deconvoluted XPS peaks, including the $sp^2$ bonding C=C at 283.5 eV, the $sp^3$ bonding C−C at 284.6 eV, the C−O at 286.1−286.6 eV, and the C=O at 288.3 eV[4,5]. However, the CKB-3 and CKB-4 only compose of three deconvoluted XPS peaks except the C=C bond. In return, the molar percentage of C−C significantly increased from 56.8% in the CKB-2 to the 66.4% in the CKB-3 (**Supplementary Table 1**). The differential (9.6%) is close to the lost C=C (12.0%). Therefore, it is reasonable to speculate that the C=C bonds are mostly converted to the C−C bonds at high concentration of sulfuric acid. In addition, the deconvoluted O 1s XPS peaks in **Supplementary Fig. 6b** at 532 and 533.4 eV are attributed to the C=O and C−O bonds, respectively[6]. The molar ratio of C−O reduced to 45.5% in the CKB-4 from 72.7% in the CKB-1. It is noticeable that the declined C−O component is

converted to the C=O bonds. In summary, the C=C and C−O bonds prefer to be converted to the C−C and C=O bonds in the case where high concentration of sulfuric acid is used for carbonization.

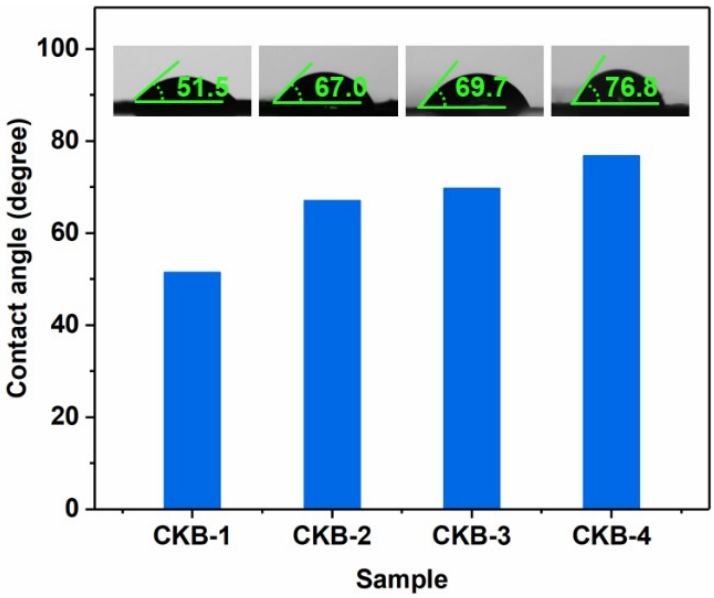


**Supplementary Figure 7.** Contact angle measurement of deionized water for the CKB catalysts.

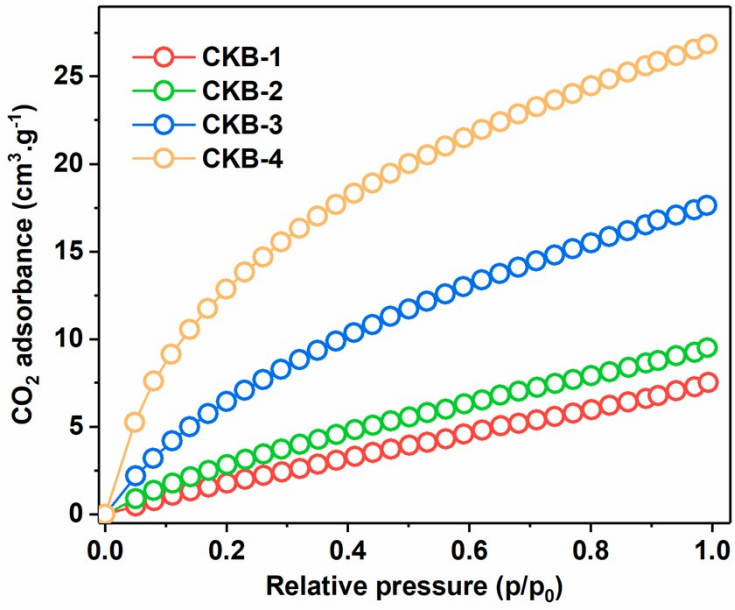


**Supplementary Figure 8.** $CO_2$ adsorption curve of the CKB photocatalysts at 273 K.

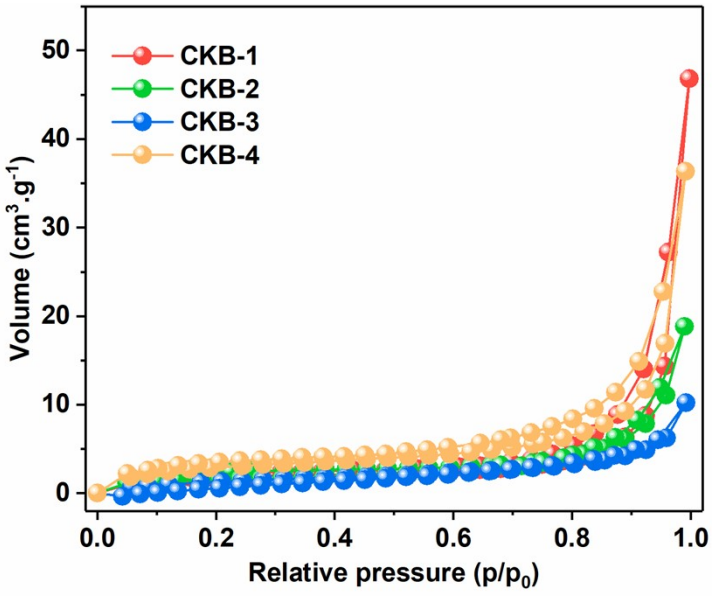


**Supplementary Figure 9.** $N_2$ adsorption-desorption isotherms of the CKB photocatalysts.

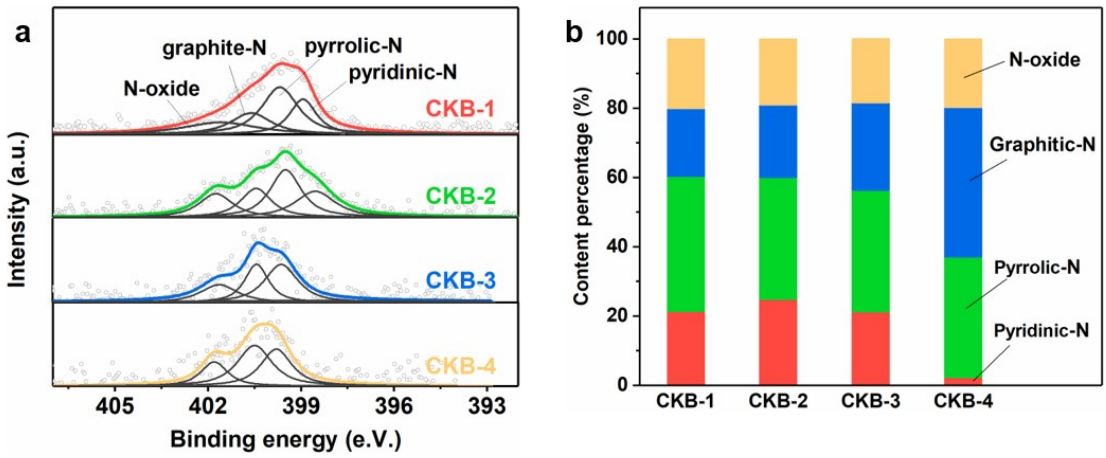


**Supplementary Figure 10.** a) The N 1s XPS spectra and b) summary of various N atomic contents for the CKB catalysts.

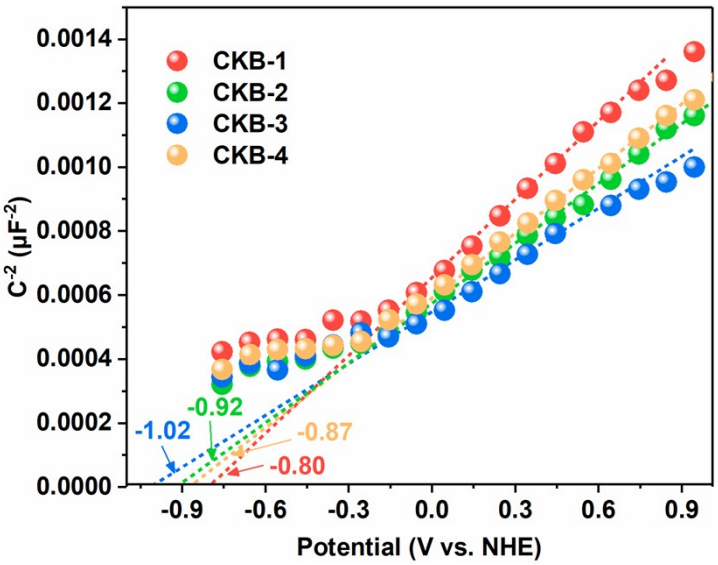


**Supplementary Figure 11**. Mott-Schottky plot for the CKB photocatalysts.

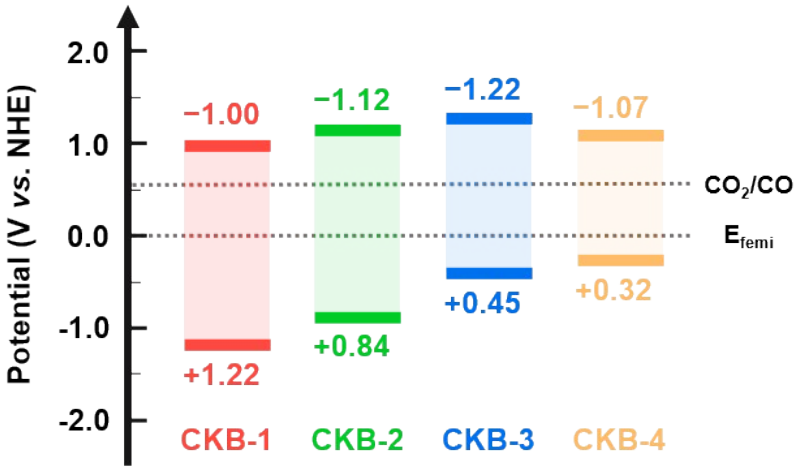


**Supplementary Figure 12**. The energy band diagram of the CKB photocatalysts.

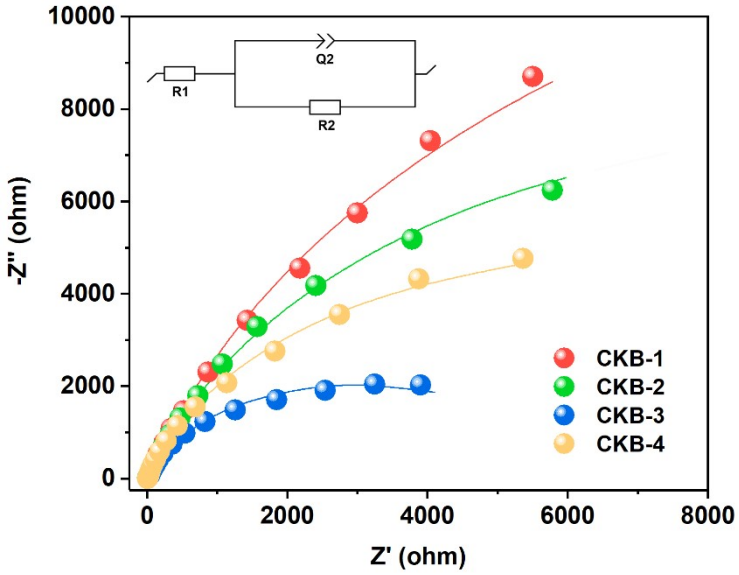


**Supplementary Figure 13.** EIS spectra at −0.4 V bias potential *vs.* SCE in 0.5 M $Na_2SO_4$ for the CKB samples.

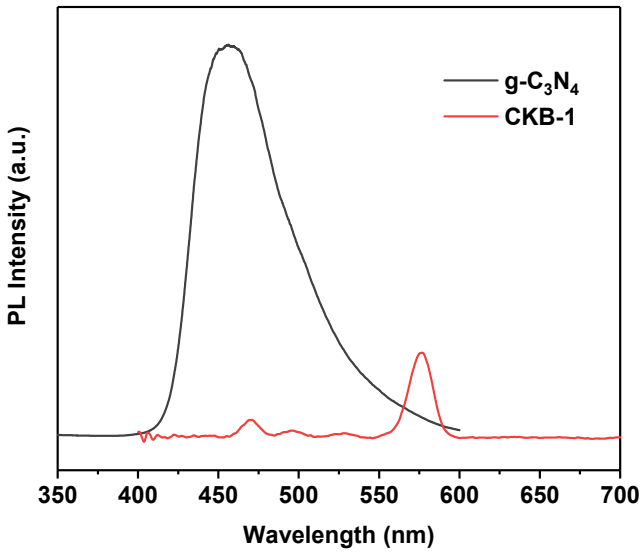


**Supplementary Figure 14.** Photoluminescence spectra of the g-$C_3N_4$ and CKB-1.

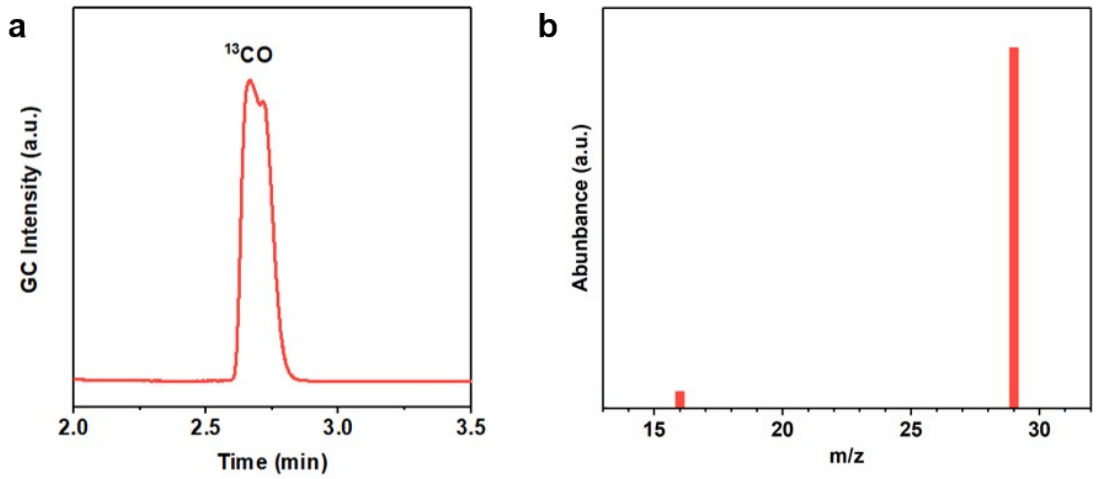


**Supplementary Figure 15.** GC-MS spectra of gaseous samples from the reaction system using the CKB-3 as the photocatalysts and $^{13}CO_2$ as the carbon source: a) GC spectrum, b) MS spectrum.

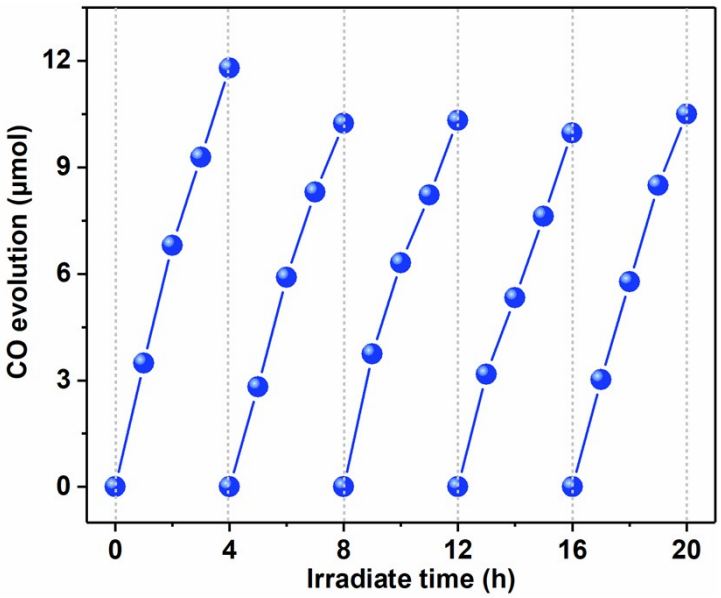


**Supplementary Figure 16.** Stability test for the photocatalytic $CO_2$ conversion performance of the CKB-3 sample (50 mg of the CKB-3 are used).

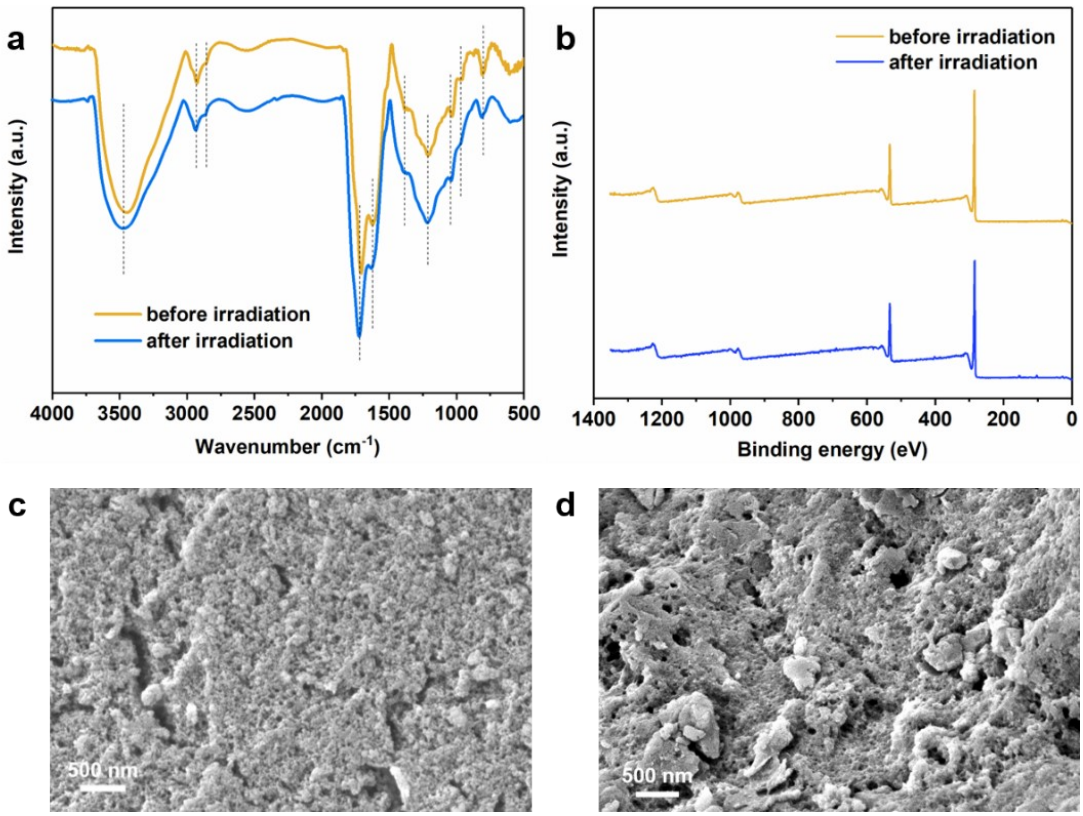


**Supplementary Figure 17.** a) FT-IR and b) XPS spectra of the CKB-3 before and after irradiation. SEM images of the CKB c) before and d) after irradiation.

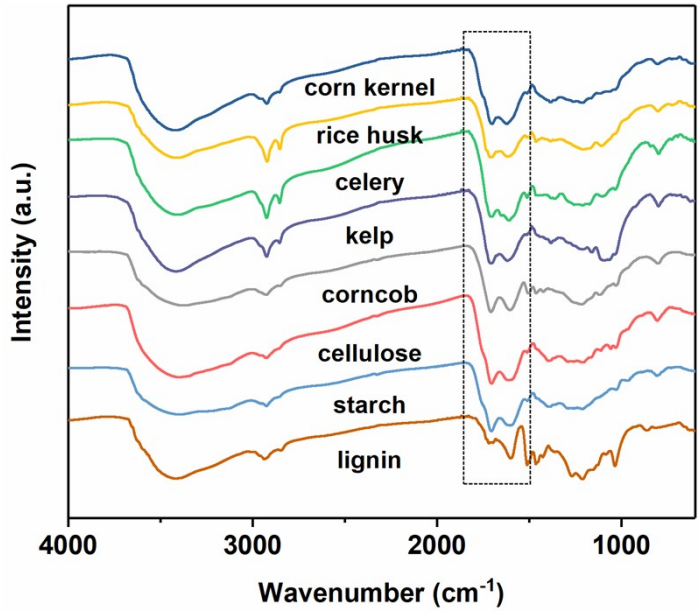


**Supplementary Figure 18.** FT-IR spectra of the carbonaceous photocatalysts derived from various biological precursors.

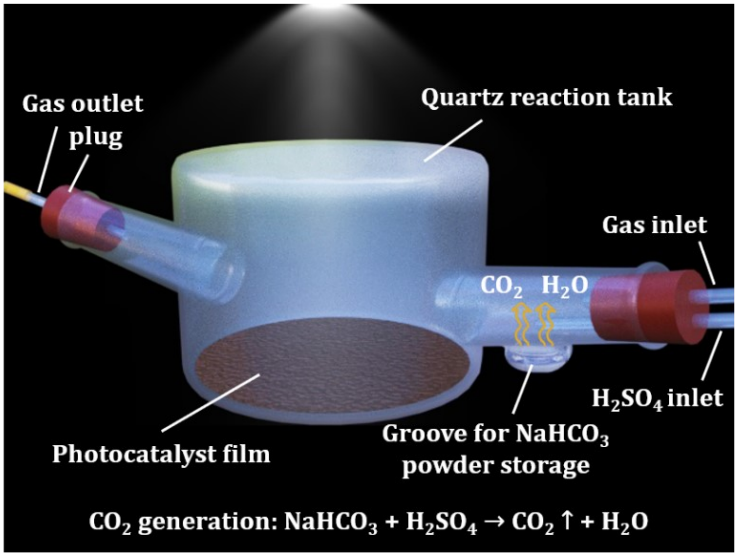


**Supplementary Figure 19.** Illustration of the gas-closed experimental reactor for photocatalytic $CO_2$ reduction in this study.

**Supplementary Table**

**Supplementary Table 1.** Element composition of the CKB photocatalysts and different chemical states of the C and O elements based on XPS spectra*

| | C 1s | | | O 1s | | | C | O | N | O/C |
|---|---|---|---|---|---|---|---|---|---|---|
| | C=C | C−C | C−O | C=O | C−O | C=O | | | | |
| CKB-1 | 25.5% | 42.4% | 27.9% | 4.2% | 72.7% | 27.3% | 73.8% | 24.5% | 1.7% | 0.33 |
| CKB-2 | 12.0% | 56.8% | 26.8% | 4.4% | 67.4% | 32.6% | 74.9% | 23.3% | 1.8% | 0.32 |
| CKB-3 | -- | 66.5% | 26.8% | 6.7% | 49.0% | 51.0% | 80.7% | 18.2% | 1.2% | 0.23 |
| CKB-4 | -- | 65.3% | 28.5% | 6.2% | 45.5% | 54.5% | 81.3% | 17.6% | 1.1% | 0.22 |

* The percentage values on the table are the atom percent.

**Supplementary Table 2.** Contents* of the typical metal impurities from natural biomass in the CKB determined by ICP-OES.

| Catalyst | $K^+$ | $Na^+$ | $Mg^{2+}$ | $Ca^{2+}$ |
|---|---|---|---|---|
| CKB-1 | 0.072% | 0.048% | 0.032% | 0.043% |
| CKB-2 | 0.066% | 0.032% | 0.029% | 0.037% |
| CKB-3 | 0.033% | 0.019% | 0.023% | 0.028% |
| CKB-4 | 0.026% | 0.018% | 0.019% | 0.017% |

*Content in the table means mass percentage, and is calculated based on the equation:

$$\text{Mass percentage} = \frac{\text{mass of the metals}}{\text{mass of the CKB catalyst}} \times 100$$

**Supplementary Table 3.** Comparation of BET surface, maximum $CO_2$ adsorption capacities, and normalized $CO_2$ adsorption capacities between the CKBs and published photocatalysts.

| Catalysts | Temperature (K) | BET surface ($m^2/g$) | Maximum $CO_2$ adsorption ($cm^3/g$) | Normalized $CO_2$ adsorption ($cm^3/m^2$) | Ref. |
|---|---|---|---|---|---|
| CKB-1 | 273 | 6.4 | 7.5 | 1.17 | This work |
| CKB-2 | 273 | 7.9 | 9.5 | 1.20 | This work |
| CKB-3 | 273 | 5.5 | 17.6 | 3.24 | This work |
| CKB-4 | 273 | 10.6 | 26.8 | 2.52 | This work |
| $La_2O_3/LaTiO_2N$ | 273 | 6.1−15.7 | 1.2−1.6 | 0.1−0.2 | [7] |
| SiC-NW/C | 273 | 470.0 | 41.5 | 0.090 | [8] |
| Ni-SA-5/$ZrO_2$ | 273 | 19.1 | 1.8 | 0.094 | [9] |
| TD-COF | 273 | 935.7 | 49.2 | 0.05 | [10] |
| Melon polymer | 273 | 118 | 15.8 | 0.13 | [11] |
| PEosinY-1 | 273 | 445 | 19.9 | 0.04 | [12] |
| $Zn_2GeO_4$/ZIF-8 | 273 | 319.5 | 15.5 | 0.05 | [13] |
| Cu/g-$C_3N_4$ foam | 273 | 9.8 | 5.4 | 0.55 | [14] |
| $Co_6$-MOF | 273 | 1957.5 | 55.2 | 0.03 | [15] |
| $ZnIn_2S_4$/N-graphene | 273 | 89 | 8.8 | 0.1 | [16] |

**Supplementary Table 4.** Fitting parameters of Raman spectra for the CKB photocatalysts.

| | P-peak | | D-peak | | Am-peak | | G-peak | | $I_D/I_G$ | $R^2$ |
|---|---|---|---|---|---|---|---|---|---|---|
| | Peak position ($cm^{-1}$) | Area percentage | Peak position ($cm^{-1}$) | Area percentage | Peak position ($cm^{-1}$) | Area percentage | Peak position ($cm^{-1}$) | Area percentage | | |
| CKB-1 | 1183 | 13.6% | 1341 | 44.7% | 1480 | 16.6% | 1579 | 25.1% | 1.78 | 0.990 |
| CKB-2 | 1192 | 16.9% | 1345 | 46.1% | 1485 | 12.6% | 1582 | 24.4% | 1.88 | 0.992 |
| CKB-3 | 1194 | 17.1% | 1344 | 51.4% | 1501 | 9.2% | 1581 | 22.3% | 2.30 | 0.995 |
| CKB-4 | 1198 | 17.3% | 1337 | 48.4% | 1480 | 10.3% | 1578 | 24.0% | 2.02 | 0.994 |

**Supplementary Table 5**. EIS fitting parameters from an equivalent circuit according to the chi-square ($\chi^2$) criterion.

| | $R_1$ (ohm·cm$^{-2}$) | $R_2$ (ohm·cm$^{-2}$) | $Q_2$ (μF·cm$^{-2}$) | $\chi^2$/\|Z\| |
|---|---|---|---|---|
| CKB-1 | 85.05±0.94 | 57474±15.78 | 194.8±0.09 | 0.066 |
| CKB-2 | 7.47±0.35 | 19358±16.63 | 103.1±0.08 | 0.026 |
| CKB-3 | 17.02±0.44 | 6002±2.52 | 236.7±0.09 | 0.096 |
| CKB-4 | 8.40±0.30 | 12114.9±12.28 | 131.0±0.15 | 0.098 |

**Supplementary Table 6**. Comparison of the photocatalytic $CO_2$ conversion performance in similar reaction systems on different photocatalysts.

| Photocatalyst | Light source | CO yield rate ($\mu mol.g^{-1}.h^{-1}$) | Ref. |
|---|---|---|---|
| CKB-1 | 300 W Xenon lamp | 51.0 | This work |
| CKB-2 | 300 W Xenon lamp | 75.1 | This work |
| CKB-3 | 300 W Xenon lamp | 115.5 | This work |
| CKB-4 | 300 W Xenon lamp | 65.3 | This work |
| Treated raped pollen | 300 W Xenon lamp | 488.4 | [17] |
| Hydrochar | 300 W Xenon lamp | 148~382 | [18] |
| SiC/C | 300 W Xenon lamp | 5.9 | [8] |
| Eosin Y-modified COPs | 300 W Xenon lamp (with a 420 nm cut-filter) | 33.0 | [12] |
| Porphyrin–tetrathiafulvalene COFs | 300 W Xenon lamp (with cut-filter to ensure the light of 420-800 nm) | 2.06 | [19] |
| Commercial g-$C_3N_4$ | 300 W Xenon lamp | 44.4 | This work |
| Commercial $TiO_2$ | 300 W Xenon lamp | 22.2 | This work |
| Commercial $WO_3$ | 300 W Xenon lamp | 11.0 | This work |
| Defective $Bi_2MoO_6$ | 300 W Xenon lamp | 3.62 | [20] |
| Oxygen-deficient BiOBr | 300 W Xenon lamp (with a 400 nm cut-filter) | 87.4 | [21] |
| $Co_3O_4$ | 200 W Xe lamp (with a standard AM 1.5 filter) | 46.3 | [22] |
| Oxygen-vacancy-$Sr_2Bi_2Nb_2TiO_{12}$ | 300 W Xenon lamp | 17.1 | [23] |

## References


1 L. Zhao, W. Li, A. Plog, Y. Xu, G. Buntkowsky, T. Gutmann and K. Zhang, *Phys. Chem. Chem. Phys.*, 2014, **16**, 26322–26329.

2 I. Van Zandvoort, E. J. Koers, M. Weingarth, P. C. A. Bruijnincx, M. Baldus and B. M. Weckhuysen, *Green Chem.*, 2015, **17**, 4383–4392.

3 R. Demir-Cakan, N. Baccile, M. Antonietti and M. M. Titirici, *Chem. Mater.*, 2009, **21**, 484–490.

4 N. Chen, Y. Huang, X. Hou, Z. Ai and L. Zhang, *Environ. Sci. Technol.*, 2017, **51**, 11278–11287.

5 N. Dwivedi, R. J. Yeo, Z. Zhang, C. Dhand, S. Tripathy and C. S. Bhatia, *Adv. Funct. Mater.*, 2016, **26**, 1526–1542.

6 J. Zhao, Y. Li, J. Mao, Y. He and J. Luo, *Tribol. Int.*, 2017, **116**, 303–309.

7 L. Lu, B. Wang, S. Wang, Z. Shi, S. Yan and Z. Zou, *Adv. Funct. Mater.*, 2017, **27**, 1–11.

8 W. Weng, S. Wang, W. Xiao and X. W. Lou, *Adv. Mater.*, 2020, **32**, 1–6.

9 X. Xiong, C. Mao, Z. Yang, Q. Zhang, G. I. N. Waterhouse, L. Gu and T. Zhang, *Adv. Energy Mater.*, 2020, **10**, 1–8.

10 H. Zhong, R. Sa, H. Lv, S. Yang, D. Yuan, X. Wang and R. Wang, *Adv. Funct. Mater.*, 2020, **30**, 2–9.

11 P. Yang, H. Zhuzhang, R. Wang, W. Lin and X. Wang, *Angew. Chemie - Int. Ed.*, 2019, **58**, 1134–1137.

12 X. Yu, Z. Yang, B. Qiu, S. Guo, P. Yang, B. Yu, H. Zhang, Y. Zhao, X. Yang, B. Han and Z. Liu, *Angew. Chemie - Int. Ed.*, 2019, **58**, 632–636.

13 Q. Liu, Z. X. Low, L. Li, A. Razmjou, K. Wang, J. Yao and H. Wang, *J. Mater. Chem. A*, 2013, **1**, 11563–11569.

14 Z. Sun, W. Fang, L. Zhao and H. Wang, *Appl. Surf. Sci.*, 2020, **504**, 144347.

15 J. Zhao, Q. Wang, C. Sun, T. Zheng, L. Yan, M. Li, K. Shao, X. Wang and Z. Su, *J. Mater. Chem. A*, 2017, **5**, 12498–12505.

16 Y. Xia, B. Cheng, J. Fan, J. Yu and G. Liu, *Sci. China Mater.*, 2020, **63**, 552–565.

17 Z. Jiang, H. Sun, T. Wang, B. Wang, W. Wei, H. Li, S. Yuan, T. An, H. Zhao, J. Yu and P. K. Wong, *Energy Environ. Sci.*, 2018, **11**, 2382–2389.

18 Z. Hu and W. Liu, *ACS Appl. Mater. Interfaces*, 2020, **12**, 51366–51373.

19 M. Lu, J. Liu, Q. Li, M. Zhang, M. Liu, J. L. Wang, D. Q. Yuan and Y. Q. Lan, *Angew. Chemie - Int. Ed.*, 2019, **58**, 12392–12397.

20 J. Di, X. Zhao, C. Lian, M. Ji, J. Xia, J. Xiong, W. Zhou, X. Cao, Y. She, H. Liu, K. P. Loh, S. J. Pennycook, H. Li and Z. Liu, *Nano Energy*, 2019, **61**, 54–59.

21 J. Wu, X. Li, W. Shi, P. Ling, Y. Sun, X. Jiao, S. Gao, L. Liang, J. Xu, W. Yan, C. Wang and Y. Xie, *Angew. Chemie - Int. Ed.*, 2018, **57**, 8719–8723.

22 L. Wang, J. Wan, Y. Zhao, N. Yang and D. Wang, *J. Am. Chem. Soc.*, 2019, **141**, 2238–2241.

23 H. Yu, J. Li, Y. Zhang, S. Yang, K. Han, F. Dong, T. Ma and H. Huang, *Angew. Chemie - Int. Ed.*, 2019, **58**, 3880–3884.